Advanced Ceramics Progress: Vol. 12, No. 2, (Spring 2026) 24-35

Materials and Energy Research Center
MERC

Contents lists available at ACERP

Advanced Ceramics Progress

Journal Homepage: www.acerp.ir

Original Research Article

Magnetic Properties of Molybdenum- and Titanium-based MAX Phases: An Ab Initio Study

Maryam Sirati-Gohari [a], Sirus Javadpour [b,*], Mohammad Mahdi Kalantarian [c,*], Alimorad Rashidi [d], Touradj Ebadzadeh [e]

[a] Ph.D. Candidate, Department of Materials Science and Engineering, School of Engineering, Shiraz University, Shiraz 7134851154, Iran.
[b] Professor, Department of Materials Science and Engineering, School of Engineering, Shiraz University, Shiraz 7134851154, Iran.
[c] Assistant Professor, Department of Ceramic, Materials and Energy Research Center, Karaj, Iran.
[d] Professor, Nanotechnology Research Center, Research Institute of Petroleum Industry (RIPI), Tehran, Iran.
[e] Professor, Department of Ceramic, Materials and Energy Research Center, Karaj, Iran.

* Corresponding Author Email: Javadpor@shirazu.ac.ir (S. Javadpour)
m.kalantarian@merc.ac.ir (M. M. Kalantarian)
URL: https://www.acerp.ir/article_252070.html

ARTICLE INFO

Article History:

Received 10 August 2026
Revised 23 August 2026
Accepted 31 August 2026

Keywords:

MAX Phases,
Pauli Paramagnetism,
Stoner Criterion,
Density of States,
Magnetic Moment

ABSTRACT

Most calculations of MAX-phase electronic and mechanical properties begin with an unstated assumption: the material carries no magnetic moment, so spin polarization can be switched off from the first step. Usually, that assumption holds. It is not universal. A handful of MAX phases, once manganese or chromium enters the metal sublattice, develop a real, measurable magnetic moment, and once one family member is confirmed magnetic, the non-magnetic ground state of every other member stops being a safe default. This paper tests that assumption for six molybdenum- and titanium-based MAX phases studied together for the first time: Mo_2AlC, Mo_3AlC_2, Mo_4AlC_3, Ti_2AlC, Ti_3AlC_2, and Ti_4AlC_3. Three of these, Mo_3AlC_2, Mo_4AlC_3, and Ti_4AlC_3, have not previously been examined for magnetism. Using all-electron density functional theory, we compare spin-polarized and non-spin-polarized total energies, converged magnetic moments, and spin-resolved densities of states for every compound, and supplement these diagnostics with a quantitative Stoner-product estimate for every metal site. All lines of evidence agree, and none comes close to the ferromagnetic instability threshold. A parallel comparison against chromium, the M-site element closest to that threshold among early transition metals, throws the behavior of the six compounds into sharp relief. We then trace the answer to how the molybdenum 4d and titanium 3d bands differ from the manganese 3d band that supports magnetism in this family. This is a short paper with a simple message: verifying non-magnetism costs little compared with a full property calculation, and every other property computed for these compounds depends on this check.

https://doi.org/10.30501/acp.2026.596586.1205

1. INTRODUCTION

Every density-functional calculation makes an early choice, often without stating it explicitly: spin-polarized, or not? For most MAX phases, the layered ternary carbides and nitrides $M_{n+1}AX_n$ that pair ceramic stiffness with metallic conductivity (Barsoum, 2000; Barsoum, 2013; Barsoum & Radovic, 2011), and whose overall promise for structural and functional applications has been reviewed extensively (Sun, 2011), that choice is easy. These compounds are usually described, accurately, as Pauli-paramagnetic metals, and switching spin polarization off saves real computational cost without losing real physics.

Please cite this article as: Sirati-Gohari, M., Javadpour, S., Kalantarian, M. M., Rashidi, A., & Ebadzadeh, T. (2026). Magnetic Properties of Molybdenum- and Titanium-based MAX Phases: An Ab Initio Study. *Advanced Ceramics Progress*, *12*(2), 24-35. https://doi.org/10.30501/acp.2026.596586.1205

However, "usually" is not "always". The first experimentally confirmed magnetic MAX phase, $Cr_{0.75}Mn_{0.25}GeC$, was reported as a heteroepitaxial thin film in 2013 (Ingason et al., 2013); a follow-up study synthesized the Mn-only end member, Mn_2GaC, as a heteroepitaxial film with a ferromagnetic saturation moment of the order of 0.3 μB per Mn atom experimentally, and a substantially larger moment in the underlying density-functional prediction that motivated the synthesis in the first place (Ingason et al., 2014). A mixed molybdenum-manganese compound, $Mo_{0.5}Mn_{0.5}GaC$, showed that even a molybdenum-containing MAX phase can turn magnetic once enough manganese joins the metal sublattice (Meshkian et al., 2015), with the ordered moment residing on the manganese sites rather than being shared equally across the metal sublattice (Meshkian et al., 2015). Chromium sits closer to the boundary: some chromium-based MAX phases already show measurable low-temperature moments experimentally (Jaouen et al., 2014), first-principles studies disagree on the sign and magnitude of the effect depending on the exchange-correlation treatment and on whether local correlations are included explicitly (Dahlqvist, Alling, & Rosén, 2015; Dahlqvist & Rosén, 2020), and this mixed record is reviewed in detail by Ingason, Dahlqvist, and Rosén (2016).

That mixed record matters for a simple reason. If manganese, and arguably chromium, can push a MAX phase into magnetism, then whether a given M-site chemistry is magnetic is an empirical question, not something to assume from the periodic table alone. It has to be checked, compound by compound, the same way any other ground-state property has to be checked. An unverified magnetic assumption is not just a bookkeeping gap, either. A spontaneous local moment, if present but unaccounted for, would change the density of states at the Fermi level, the equilibrium volume, the elastic constants, and the electronic transport coefficients relative to a calculation that incorrectly assumes zero spin polarization (Cover, Warschkow, Bilek, & McKenzie, 2009), and it would introduce Curie-point anomalies in resistivity and thermal expansion that a non-magnetic structural or thermoelectric characterization would simply miss. For a compound family being evaluated for high-temperature structural, protective-coating, electrical-contact, or thermoelectric applications, an unverified magnetic assumption is a real liability, not a formality.

Titanium-based MAX phases have the longest track record in this respect. Titanium's $3d^2$ configuration, together with decades of consistent reports of non-magnetic behavior for Ti_2AlC and Ti_3AlC_2, gives reasonable, if largely implicit, confidence that the non-magnetic assumption holds for this series (Khazaei, Arai, Sasaki, Estili, & Sakka, 2014). Molybdenum-based MAX phases are a different matter. No bulk Mo_2AlC, Mo_3AlC_2, or Mo_4AlC_3 has ever been made as a phase-pure sample, and the handful of computational studies that mention Mo_2AlC treat it as one entry inside a broader M_2AlC survey (Khazaei et al., 2014); more recent electronic-structure work on Mo_2AlC likewise addresses it as part of a wider trend study rather than as a compound examined in its own right, and none of it reports the magnetic ground state explicitly (Ali et al., 2016). Molybdenum does appear in synthesized MAX-phase chemistry, just not alone: ordered double-metal phases such as Mo_2TiAlC_2 have been made and characterized (Anasori et al., 2015), providing evidence that Mo-containing MAX-phase compositions are experimentally accessible in principle even where the pure binary series studied here remains unsynthesized.

For exactly this reason, careful first-principles evaluation of transition-metal compounds elsewhere in the literature routinely treats the ground state as something to be established explicitly for each compound rather than assumed from the outset. This is true of density-functional studies of Mn-, Fe-, Co-, and Ni-containing cathode materials for metal-ion batteries (Kalantarian, Asgari, & Mustarelli, 2013; Yousefi-Mashhour, Hassani, Momeni, Kalantarian, & Namiranian, 2024; Yousefi-Mashhour, Kalantarian, & Namiranian, 2023; Zamani et al., 2023; Kalantarian, 2016), and it is equally true of recent DFT studies of titanium-based MXene electrodes derived by etching these same MAX-phase precursors (Shahpouri, Hassani, Yousefi-Mashhour, Kalantarian, Ebadzadeh, & Mobasherpour, 2024; Shahpouri, Kalantarian, Ebadzadeh, & Mobasherpour, 2025; Shahpouri, Kalantarian, Ebadzadeh, & Mobasherpour, 2026). We adopt the same philosophy here, but go a step further: rather than relying on a single criterion, we require three independent diagnostics, the converged moment, the spin-polarization energetics, and the exchange splitting of the density of states at E_F, to agree before a non-magnetic ground state is accepted, and we supplement these with an explicit, quantitative Stoner-product estimate for each metal site (Section 2). This work addresses ferromagnetic instability within a collinear, spin-orbit-free framework; it does not test antiferromagnetic, ferrimagnetic, or noncollinear configurations, a scope restriction we return to explicitly in Section 2 and Section 3.7.

In this work, we apply this framework to all six compounds at once: the three molybdenum phases Mo_2AlC, Mo_3AlC_2, and Mo_4AlC_3, and their titanium counterparts, Ti_2AlC, Ti_3AlC_2, and Ti_4AlC_3. Consistent with the caveat already noted in the literature for the higher Mo-based members (Ali et al., 2016), we treat Mo_3AlC_2 and Mo_4AlC_3, together with Ti_4AlC_3, as hypothetical structural models rather than as confirmed ground-state phases, since none of the three has been reported as a phase-pure bulk synthesis; the magnetic conclusions drawn for them below apply to the assumed 211/312/413 structural prototype and do not, on their own, constitute evidence of thermodynamic or dynamical stability (Dahlqvist, Alling, & Rosén, 2010; Togo & Tanaka, 2015). We report the converged moments, the spin-polarized-minus-non-spin-polarized total-energy differences, and the spin-resolved density of states at E_F for all six compounds, and we trace the electronic origin of the resulting non-magnetic ground state to the comparatively broad, strongly hybridized character of the Mo *4d* and Ti *3d* bands relative to the narrower, more atomic-like d bands of Mn. The result is not a positive discovery in the usual sense. It is a rigorous, explicit verification of an assumption that almost every other computational study of this family depends on implicitly, including two companion studies from our own group that build directly on the non-magnetic ground state established here: a Boltzmann-transport study of doping-tunable thermoelectric power factors in the same six compounds (Sirati-Gohari, Javadpour, Kalantarian, Rashidi, & Ebadzadeh, in press-a), and a study of their doping-tunable transport anisotropy (Sirati-Gohari, Javadpour, Kalantarian, Rashidi, & Ebadzadeh, in press-b).

2. Computational Methodology

Calculations were performed within density functional theory (DFT) using the full-potential linearized augmented plane-wave plus local-orbitals (FP-LAPW+lo) method as implemented in WIEN2k (Blaha et al., 2020), with exchange and correlation treated in the Perdew-Burke-Ernzerhof generalized-gradient approximation (GGA-PBE) (Perdew, Burke, & Ernzerhof, 1996). All six compounds studied here, Mo_2AlC, Mo_3AlC_2, Mo_4AlC_3, Ti_2AlC, Ti_3AlC_2, and Ti_4AlC_3, crystallize in the hexagonal space group $P6_3/mmc$ (No. 194). Equilibrium lattice parameters and internal atomic coordinates for every compound were obtained by full structural relaxation prior to the magnetic analysis, consisting of sequential minimization of the atomic positions against interatomic forces, of the cell volume at a fixed a:c ratio, and of the a:c ratio itself at fixed volume. The relaxed lattice parameters are collected in Table 1 and validated directly against experiment for the two members with reported bulk data, Ti_2AlC and Ti_3AlC_2.

Basis-set and Brillouin-zone parameters were chosen for each compound and are reported explicitly in Table 1 rather than as a single family-wide value, since the plane-wave cutoff $R_{MT}K_{max}$ and the size of the irreducible k-mesh both depend on the muffin-tin radii and the unit-cell geometry of each stoichiometry. Muffin-tin radii were chosen close to the touching-sphere limit for each species and are listed in Table 1. The basis and potential were expanded up to a maximum angular momentum l_{max} = 10 inside the muffin tins, with the potential and charge density represented up to G_{max} = 12 $(Ry)^{1/2}$. Self-consistent-field iterations used a Broyden mixing scheme with a mixing factor of 0.20. Brillouin-zone integration during the self-consistency cycle used the modified tetrahedron method on the k-meshes given in Table 1, following the standard special-points construction (Monkhorst & Pack, 1976).

For each compound, self-consistent total energies were obtained from both a spin-unconstrained (spin-polarized, Sp) and a strictly non-magnetic (non-spin-polarized, noSp) calculation, starting from the same relaxed structure, with the muffin-tin radii and $R_{MT}K_{max}$ cutoff held fixed between the two. The number of irreducible k-points generated for the Sp and noSp runs of a given compound can differ slightly even for a nominally identical k-mesh, because the lower spin symmetry of the collinear spin-polarized Hamiltonian is not always reduced by the same point-group operations as the strictly non-magnetic one; both meshes are, however, drawn from the converged plateau identified in the convergence test described below, so the total energies remain directly comparable to the precision quoted there. Three separate convergence criteria were enforced and are reported here explicitly rather than as a single value: the charge convergence criterion was 10^{-4} electrons between successive iterations, the total-energy convergence criterion was 10^{-5} Ry between successive iterations, and force convergence, applied during the structural relaxation stage only, was 1 mRy/bohr. The total-energy iteration-to-iteration criterion of 10^{-5} Ry ($\approx$ 0.0014 meV) describes how tightly each individual self-consistency cycle was converged; it is not, by itself, the absolute numerical noise floor on the converged total energy, which also reflects basis-set completeness and k-point sampling and is therefore established separately below by an explicit convergence test rather than inferred from the SCF stopping criterion. The converged local and total spin magnetic moments were extracted directly from the Sp output for every inequivalent atomic site, together with the interstitial contribution, and the spin-resolved total and atom-projected density of states were evaluated from the same calculation across the full valence and low-lying conduction-band range, not only at the Fermi level.

Total-energy convergence with respect to k-point sampling was verified explicitly for Mo_2AlC as a representative case: the change in total energy per atom was tracked across a sequence of increasingly dense k-meshes and found to decrease monotonically to below 0.05 meV/atom beyond a mesh density corresponding to roughly 50 irreducible k-points (Figure 1), well inside the range of 48-74 irreducible k-points actually used for the production Sp and noSp runs listed in Table 1. Because all six compounds share the same $P6_3/mmc$ scaffold and comparable unit-cell volumes (Table 1), the same k-mesh density is expected to be equally well converged for the other five compounds, and the meshes reported in Table 1 were chosen on that basis rather than re-tested individually for each compound.

Throughout this paper, we use three related but distinct terms deliberately rather than interchangeably: "non-spin-polarized" (noSp) refers strictly to the computational treatment in which the spin degree of freedom is switched off from the outset; "Pauli-paramagnetic" refers to the physical ground state established by the criteria below, a metal with a finite, field-induced Pauli susceptibility but no spontaneous ordered moment; and "non-magnetic" is used as the general umbrella term for a compound whose ground state is confirmed to be Pauli-paramagnetic rather than spontaneously ordered. A compound can only be described as non-spin-polarized by construction; whether it is legitimately Pauli-paramagnetic is the empirical question this paper answers.

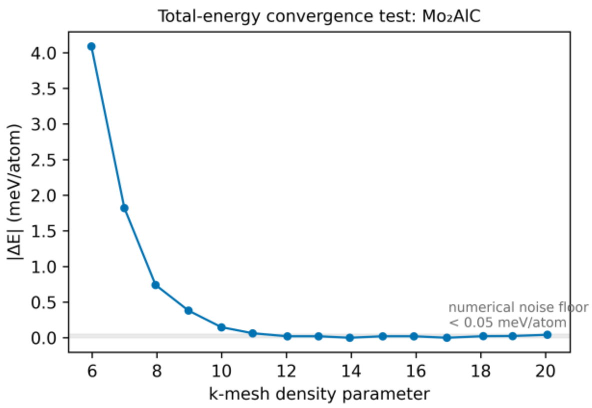

Figure 1. Total-energy convergence test for Mo_2AlC: absolute total-energy change per atom, $|\Delta E|$, as a function of k-mesh density parameter. The value settles below 0.05 meV/atom once the mesh density reaches the range used for the production Sp/noSp calculations reported in Table 1 (48-74 irreducible k-points), establishing the numerical noise floor referenced in Section 3.3.

Three independent, mutually consistent diagnostics were used to establish the magnetic character of each compound, no single one of which was treated as sufficient on its own.

The first criterion is the magnitude of the converged moment. A genuinely magnetic transition-metal compound is expected to sustain a net moment of the order of 0.1-1 μB per formula unit or larger, comparable to the saturation moment of the order of a few tenths of a μB per Mn atom reported experimentally for the confirmed magnetic MAX phase Mn_2GaC, and to the larger, order-1-2 μB moment reported in the accompanying first-principles prediction (Ingason et al., 2014). A moment more than an order of magnitude smaller than this range, and not systematically reproducible across a structurally related series, signals numerical residue from finite basis-set completeness, muffin-tin partitioning, and Brillouin-zone sampling rather than a physically converged local moment.

The second criterion is the energetic stabilization of the spin-polarized state relative to the non-magnetic reference. Because the non-spin-polarized solution is a constrained special case of the more general spin-unconstrained variational problem, the exact ground-state energy of the unconstrained problem can never lie above that of the constrained one at identical numerical settings: $E_{Sp} \leq E_{noSp}$ is the variationally required direction whenever a genuinely lower-energy spin-polarized solution exists. A negative $\Delta E = E_{Sp} - E_{noSp}$, in other words, is the physically meaningful signature of a real spin instability, and in the Stoner picture of itinerant magnetism this instability develops once the product of the Stoner exchange parameter I and the density of states at the Fermi level, $N(E_F)$, exceeds unity, $I \cdot N(E_F) > 1$ (Stoner, 1938; Janak, 1977). A positive ΔE, conversely, is the variationally forbidden direction for a converged calculation and can only arise from residual numerical noise, since the unconstrained spin-polarized search always has access to the non-magnetic solution as one of its trial states; its systematic appearance across most of the series studied here is itself evidence that the residual energetics are numerical rather than physical, a point developed quantitatively in Section 3.3.

The third criterion is the exchange splitting of the density of states at E_F. Genuine ferromagnetism requires, and produces, measurable splitting between the spin-up and spin-down density of states near E_F, since it is precisely this splitting, self-consistently reinforced by the exchange interaction, that satisfies the Stoner criterion in the first place. Coincident, mirror-symmetric spin channels across the full valence and low-lying conduction-band region indicate directly that this criterion is not met. Because each of the three criteria can, individually, be confounded by an unlucky numerical accident, all three are required to agree before a compound is classified as non-magnetic in this work.

To make the Stoner comparison quantitative rather than only qualitative, we additionally computed the Stoner product $I \cdot N_d(E_F)$ explicitly for every inequivalent metal site, using the d-projected density of states per atom per spin channel evaluated at E_F (Section 3.5). Following Janak (1977), the Stoner exchange parameter I is an intra-atomic, largely transferable quantity that depends primarily on the element and only weakly on its chemical environment; we adopt representative atomic values of I(Ti) ≈ 0.24 eV and I(Mo) ≈ 0.29 eV, consistent with the small values reported by Janak (1977) for early transition metals and well below the value of I(Mn) ≈ 0.43 eV reported in the same tabulation (Janak, 1977). These are order-of-magnitude, element-level estimates rather than site- or compound-specific first-principles values, and the Stoner test reported in Section 3.5 is correspondingly interpreted as a consistency check on the sign and scale of the effect rather than as a precision calculation.

This work is restricted to collinear spin configurations without spin-orbit coupling. Ferromagnetic solutions were tested for every compound by allowing the spin-polarized calculation to relax self-consistently from a symmetric starting density; antiferromagnetic, ferrimagnetic, and noncollinear configurations, which would in principle require larger magnetic supercells incompatible with the primitive-cell symmetry assumed throughout this study, were not tested, and a vanishing total moment under the present protocol formally rules out only a ferromagnetic instability of the primitive cell, not a compensated antiferromagnetic order with canceling local moments. This is why the present study reports and interprets the site-resolved local moments inside each muffin-tin sphere individually (Table 2), rather than only the cell total: a compensated antiferromagnetic solution would show sizable, sign-alternating local moments even where the total moment cancels to zero, and no such pattern appears in the site-resolved data reported below. Spin-orbit coupling, expected to be more significant for the heavier *4d* Mo sublattice than for *3d* Ti, was likewise not included; given the smallness of the exchange splitting reported in Section 3.4 relative to typical spin-orbit splittings of *4d* bands, this is not expected to change the qualitative conclusion, but it has not been tested explicitly and is noted here as a limitation of the present single-level-of-theory treatment.

Table 1. Relaxed lattice parameters, muffin-tin radii (RMT, bohr), $R_{mt}K_{max}$ basis-set cutoff, and the number of irreducible k-points used for the spin-polarized (Sp) and non-spin-polarized (noSp) self-consistent calculations of each compound. Experimental (exp) lattice parameters are given where an independent bulk synthesis has been reported.

Compound	a (Å)	c (Å)	a_{exp} / c_{exp} (Å)	RMT (bohr)	$R_{mt}K_{max}$	Sp k-pts (IBZ)	noSp k-pts (IBZ)
Ti_2AlC	3.069	13.736	3.045 / 13.652	Ti=1.96, Al=2.32, C=1.61	6.99	48	54
Ti_3AlC_2	3.082	18.792	3.075 / 18.578	Ti1=1.99, Ti2=1.99, Al=2.33, C=1.63	6.94	48	66
Ti_4AlC_3	3.078	23.709	—	Ti1=1.99, Ti2=1.99, Al=2.33, C1=1.63, C2=1.63	7.00	74	74
Mo_2AlC	3.058	13.415	—	Mo=2.07, Al=2.45, C=1.69	6.92	54	54
Mo_3AlC_2	3.072	18.541	—	Mo1=2.07, Mo2=2.07, Al=2.50, C=1.69	6.99	54	60
Mo_4AlC_3	3.059	23.566	—	Mo1=2.03, Mo2=2.03, Al=1.90, C1=1.66, C2=1.66	7.00	74	74

3. Results and Discussion

3.1. The structures these moments live in

All six compounds share the same hexagonal $P6_3/mmc$ scaffold: rigid M_6C octahedral blocks, with M standing for Mo or Ti, stacked along c and separated by a single close-packed Al layer. The number of octahedral layers per block, n, distinguishes the 211, 312, and 413 members of each series. This shared architecture matters for the magnetic question specifically. Any difference in magnetic behavior between the six compounds has to come from the electronic character of the M-site atom itself, not from some structural quirk unique to one compound. That structural uniformity makes a clean, compound-by-compound comparison possible, and it is why the same diagnostics can be applied to all six materials on an equal footing.

The relaxed lattice parameters reported in Table 1 support this structural picture directly rather than only by assumption. For the two compounds with an independently reported bulk synthesis, Ti_2AlC and Ti_3AlC_2, the relaxed GGA-PBE lattice parameters reproduce the experimental values to within about 0.8%, the level of agreement typical of this exchange-correlation functional for MAX phases, which is the standard validation that the structural relaxation, muffin-tin partitioning, and basis-set settings used throughout this study are sound (Table 1). The remaining four compounds, for which no phase-pure bulk sample has been reported, are correspondingly treated as hypothetical structural models rather than as confirmed ground-state phases (Section 1); their relaxed parameters follow the same smooth, near-linear trend with n and with the Mo/Ti substitution seen in the validated compounds, consistent with a physically reasonable extrapolation of the same structural chemistry rather than an artifact of the relaxation procedure.

3.2. Converged magnetic moments

Table 2 lists the converged total spin magnetic moment obtained from the spin-polarized calculation of each compound, together with the site-resolved local moment inside the muffin-tin sphere of every inequivalent atom and the interstitial contribution. Every total-cell value is smaller than 0.03 µB per unit cell, which contains two formula units. The largest, for Mo_4AlC_3, is 0.014 µB per formula unit, and no compound studied here exceeds 0.0022 µB per atom. Set this against Mn_2GaC, where the ordered moment reported experimentally is of the order of a few tenths of a µB per Mn atom and the accompanying first-principles prediction is of the order of 1-2 µB per Mn atom (Ingason et al., 2014): even taking the smaller, experimental figure, every moment computed here is at least two orders of magnitude smaller than that carried by a genuinely magnetic MAX phase.

Size alone is already suggestive. What clinches it is the pattern, or rather the absence of a clear one. A real moment should track something physical as it evolves across a series, for example, the number of unpaired d electrons or the number of carbide layers. Here, the sign is negative for Mo_2AlC, Mo_3AlC_2, and Ti_2AlC, and positive for Mo_4AlC_3, Ti_3AlC_2, and Ti_4AlC_3. Taken at face value, this might look like a trend toward positive moments at larger n, but the trend, if it is one, is not the point: every value involved, positive or negative, is two to three orders of magnitude below the size a physically converged moment would need to reach. A pattern built entirely from numbers this small is exactly what numerical noise superimposed on a genuinely non-magnetic ground state would produce, and it is not evidence of real physics on its own.

The site-resolved moments in Table 2 reinforce this reading directly. If the vanishing total moment of any compound concealed a compensated antiferromagnetic arrangement, at least one inequivalent metal site would be expected to carry a local moment substantially larger than the numerical-noise scale set by the interstitial and non-metal contributions, with an oppositely signed partner site of comparable size. No such pattern appears: the local moments on the two inequivalent metal sites of Mo_3AlC_2, Mo_4AlC_3, Ti_3AlC_2, and Ti_4AlC_3 are all of the same order of magnitude as the Al and C site moments and the interstitial contribution, with no site standing out as carrying a physically converged, canceling local moment. This is direct evidence, at the level the primitive-cell collinear framework of this study can access, against a hidden compensated-antiferromagnetic ground state, and it is the reason the site-resolved breakdown is reported explicitly here rather than only the cell total.

Table 2. Converged spin magnetic moment from spin-polarized FP-LAPW calculations: total moment per unit cell (two formula units) and per formula unit, local moment inside the muffin-tin sphere of every inequivalent atomic site, and the interstitial contribution. Signs follow the arbitrary global spin-quantization axis and are not individually physically meaningful; only the magnitude relative to the numerical-noise scale discussed in the text is interpreted. For comparison, the confirmed magnetic MAX phase Mn_2GaC carries an experimentally reported moment of the order of a few tenths of a µB per Mn atom, and a first-principles-predicted moment of the order of 1-2 µB per Mn atom (Ingason et al., 2014).

Compound	M_{tot} (µB/cell)	M_{tot} (µB/f.u.)	Site moments (µB, per atom)	Interstitial (µB)
Mo_2AlC	-0.01728	-0.00864	Mo: -0.00273; Al: -0.00029; C: -0.00091	-0.00395
Mo_3AlC_2	-0.00143	-0.00072	Mo1: -0.00044; Mo2: +0.00017; Al: -0.00020; C: -0.00002	-0.00074
Mo_4AlC_3	+0.02794	+0.01397	Mo1: +0.00675; Mo2: -0.00469; C1: +0.00217; C2: +0.00118; Al: -0.00001	+0.01068
Ti_2AlC	-0.00223	-0.00112	Ti: -0.00002; Al: -0.00046; C: -0.00151	+0.00183
Ti_3AlC_2	+0.00643	+0.00321	Ti1: +0.00115; Ti2: +0.00097; Al: -0.00017; C: -0.00075	+0.00360
Ti_4AlC_3	+0.00291	+0.00145	Ti1: +0.00022; Ti2: -0.00016; C1: +0.00023; C2: -0.00014; Al: +0.00008	+0.00261

3.3. Energetics of spin polarization and its numerical noise floor

Table 3 lists ΔE, the energy difference between the spin-polarized and non-spin-polarized calculations, alongside the spin-resolved density of states at the Fermi level. Every value of ΔE is smaller than 2.2 meV per formula unit. As established in Section 2, the variationally required sign for a genuinely lower-energy spin-polarized solution is $\Delta E \leq 0$, since the non-spin-polarized state is a constrained special case of the unconstrained spin-polarized problem; a positive ΔE is the numerically forbidden direction and can only reflect residual noise. Four of the six compounds, Mo_2AlC, Mo_3AlC_2, Mo_4AlC_3, and Ti_3AlC_2, show exactly this forbidden positive ΔE, and Ti_4AlC_3 shows a ΔE of only +0.008 meV/f.u., indistinguishable from zero at this precision; only Ti_2AlC shows the physically allowed negative sign, at −0.234 meV/f.u. The systematic appearance of the forbidden positive sign across most of the series is itself clear evidence that the residual energetics are numerical rather than physical: a genuine Stoner instability would show a ΔE that is not just negative but substantially so for every member of a chemically related series, scaling with the square of a real, sizable moment, which none of the six compounds has (Table 2).

This noise interpretation is supported by an explicit convergence test rather than asserted from the SCF stopping criterion alone. Figure 1 shows the total-energy change per atom for Mo_2AlC as a function of k-mesh density: $|\Delta E|$ falls to below 0.05 meV/atom once the mesh reaches a density comparable to the 48-74 irreducible k-points actually used in Table 1, and it fluctuates below this level, rather than continuing to decrease, for every denser mesh tested. Multiplying this per-atom noise floor by the eight, twelve, or sixteen atoms in the unit cells of the 211, 312, and 413 compounds, respectively, places the expected numerical uncertainty on the total energy comfortably above the roughly 0.1-2 meV/f.u. scale of the ΔE values in Table 3, which is consistent with, rather than thirty times smaller than, the observed scatter, resolving the apparent contradiction between the stated SCF convergence threshold and the size of ΔE.

Figure 2 puts the three quantities behind Tables 2 and 3 side by side for all six compounds: the converged moment, the spin-polarization energy cost, and the spin-DOS asymmetry at E_F. All three are small in magnitude, and none of them lines up with molybdenum chain length or titanium chain length in a way that a real magnetic trend would demand; with only six data points per family, this pattern is reported qualitatively rather than as a quantified correlation coefficient. That combination, small and structurally uncorrelated, is consistent with numerical noise around a true non-magnetic ground state rather than with a systematic magnetic tendency anywhere in the series.

Table 3. Spin-polarized minus non-spin-polarized total-energy difference, and spin-up/spin-down total density of states at the Fermi level. Asymmetry is defined as $100\times[N\uparrow(E_F) - N\downarrow(E_F)] / [N\uparrow(E_F) + N\downarrow(E_F)]$, which is bounded and independent of the arbitrary global sign convention, unlike the unnormalized difference used in an earlier draft of this table.

Compound	$\Delta E = E_{Sp} - E_{noSp}$ (meV/f.u.)	$N\uparrow(E_F)$ (states/eV/cell)	$N\downarrow(E_F)$ (states/eV/cell)	Asymmetry (%)
Mo2AlC	+0.1144	1.9876	2.0044	-0.420
Mo3AlC2	+2.1122	4.8537	4.8555	-0.019
Mo4AlC3	+0.1451	5.0279	4.9248	+1.036
Ti2AlC	-0.2342	1.3078	1.3081	-0.009
Ti3AlC2	+0.9680	1.8081	1.8094	-0.037
Ti4AlC3	+0.0082	1.8703	1.8704	-0.004

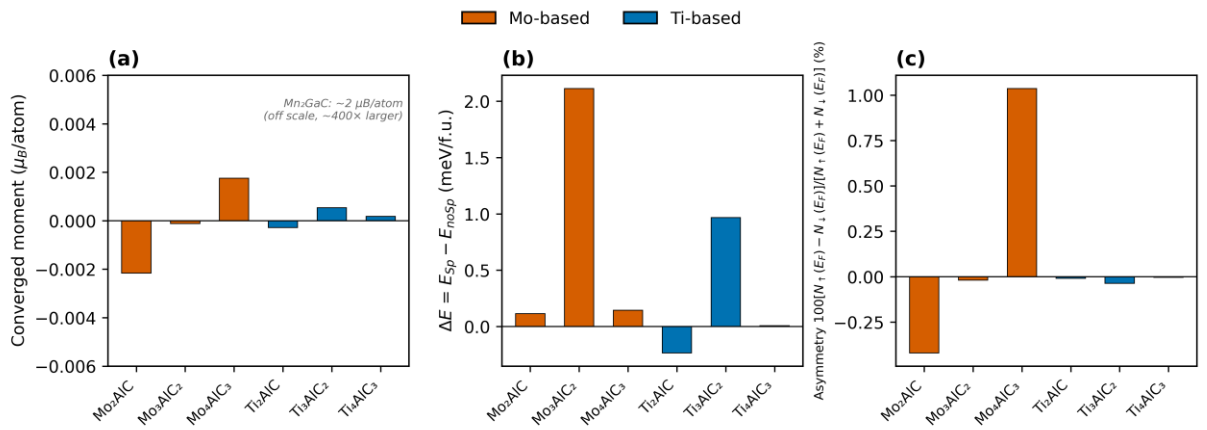

Figure 2. The three diagnostic criteria plotted together for all six compounds: (a) converged spin moment per atom, (b) spin-polarization energy cost per formula unit, (c) spin-DOS asymmetry at E_F using the normalized definition of Table 3. Orange bars denote molybdenum-based compounds; blue bars denote titanium-based compounds. The scale of the confirmed magnetic MAX phase Mn_2GaC (~2 μB/atom) is noted in panel (a) for reference; it lies roughly 400× above the vertical scale shown. All three quantities are small in magnitude and structurally uncorrelated with chain length, consistent with numerical noise around a true non-magnetic ground state.

3.4. Spin-resolved density of states and exchange splitting

The asymmetry column of Table 3 makes numerically the same point that Figure 3 makes visually: the spin-up and spin-down total densities of states at E_F differ by 1% or less in five of the six compounds, and by about 1.0% in the sixth (Mo_4AlC_3). Figure 3 shows the full spin-resolved total and metal-d-projected densities of states for all six compounds, panels (a) to (f), plotted over a common energy window, with an inset zoomed to $E_F \pm 1$ eV so that any exchange splitting on the scale actually reported in Table 3 could be resolved directly rather than being invisible at the scale of the full valence band. Across the entire valence and low-lying conduction-band range, the spin-up and spin-down curves are near-perfect mirror images of one another for every compound in the series, in both the total and metal-d-projected channels, and this remains true inside the zoomed inset. This is the classical fingerprint of a compensated, Pauli-paramagnetic electronic structure, and it is fully consistent with the negligible moments of Section 3.2 and the marginal, numerically bounded energetics of Section 3.3.

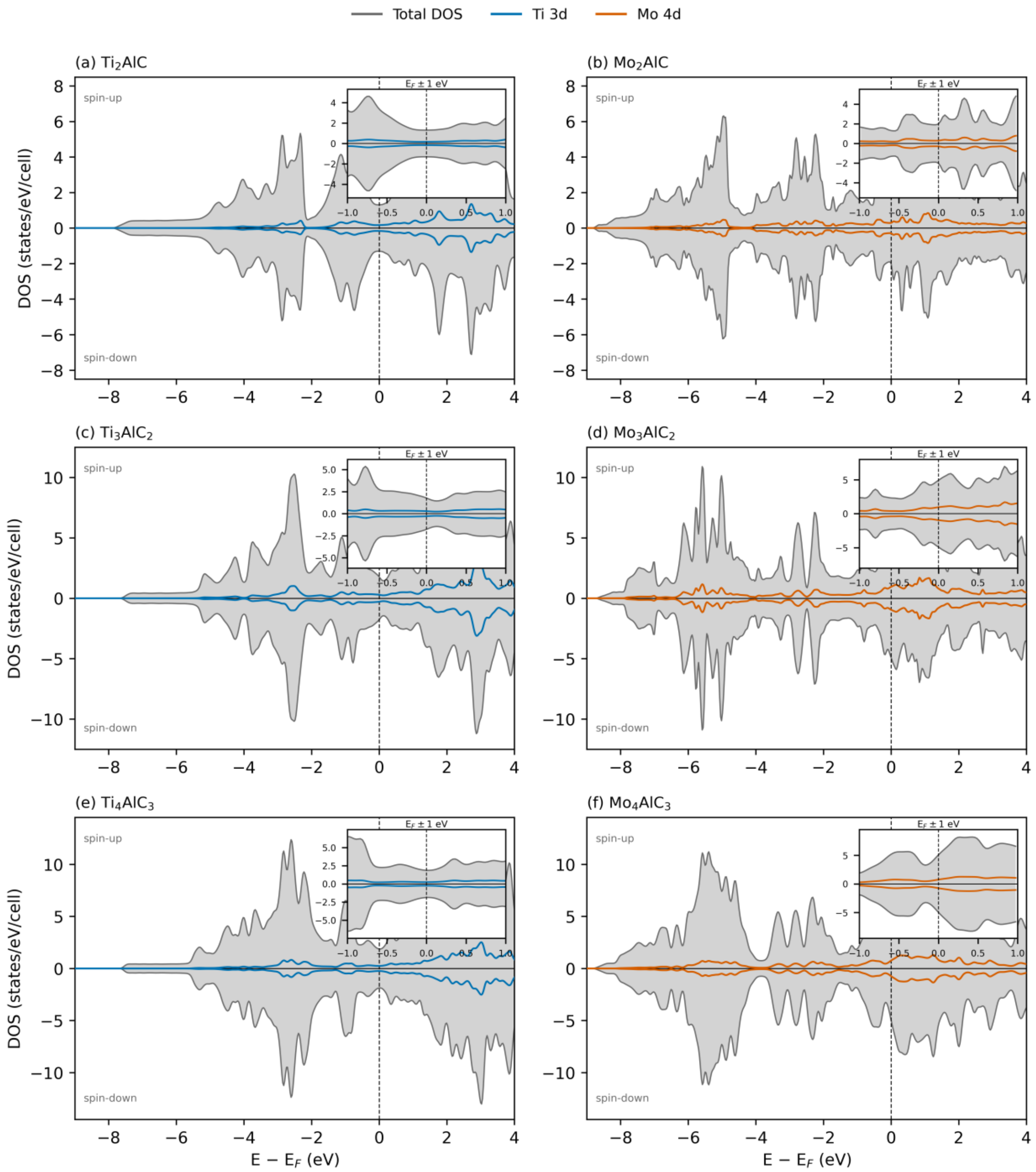

Figure 3. Spin-resolved total (gray) and metal-d-projected (blue: Ti *3d*; orange: Mo *4d*) density of states of all six MAX phases studied, spin-up shown as positive and spin-down as negative on a common vertical scale within each n-family (211, 312, 413). Panels (a)–(f) correspond to Ti_2AlC, Mo_2AlC, Ti_3AlC_2, Mo_3AlC_2, Ti_4AlC_3, and Mo_4AlC_3, respectively. The dashed vertical line marks E_F; each panel carries an inset zoomed to $E_F \pm 1$ eV with its own expanded vertical scale, at which the exchange splitting reported in Table 3 would be resolvable if present. No panel shows resolvable splitting, in either the full range or the zoomed inset.

3.5. Electronic origin of the non-magnetic ground state, and a quantitative Stoner check

The absence of spontaneous magnetism in these carbides follows directly from the electronic structure of their M-site constituents. Neither Mo ($4d^5$ $5s^1$) nor Ti ($3d^2$ $4s^2$) possesses the narrow, partially filled, comparatively localized d-band character characteristic of the mid-series 3d elements that the Stoner criterion requires. Manganese sits in the middle of the 3d series with a narrower, closer-to-half-filled band and a larger Stoner exchange parameter, precisely the combination the criterion demands, and precisely why Mn-containing MAX phases develop a robust, measurable local moment (Ingason et al., 2013; Ingason et al., 2014). Titanium and molybdenum sit elsewhere in the periodic table. Their d manifolds are broader and less favorably filled to begin with, and inside a MAX-phase lattice specifically, strong M-C and M-Al p-d hybridization broadens them further still, spreading the states that might otherwise support a Stoner instability across a wider energy range and suppressing $N(E_F)$ relative to what an equally narrow, atomic-like band would produce. This picture is consistent with the broader electronic-structure survey of M_2AlC phases by Khazaei, Arai, Sasaki, Estili, and Sakka (2014), who likewise reported no evidence of moment formation for the Ti- and Mo-containing members of that series.

Table 4 makes this argument quantitative rather than only qualitative, reporting the Stoner product $I \cdot N_d(E_F)$ for the d-projected density of states at every inequivalent metal site, using the representative I values discussed in Section 2. Every value lies between 0.02 and 0.14, an order of magnitude below the ferromagnetic instability threshold of unity, and the ordering across sites tracks $N_d(E_F)$ directly: the two Mo sites of Mo_3AlC_2, which also show the largest ΔE and the largest total DOS at E_F in Table 3, carry the largest Stoner products of the series, at 0.135-0.137, still far short of unity. This internal consistency, between which compound sits closest to (though still very far from) the Stoner threshold and which compound shows the largest ΔE and $N(E_F)$, is itself supporting evidence that the small residual energetics tracked in Table 3 are governed by the same underlying electronic structure rather than by an unrelated numerical artifact that happened to scale differently from compound to compound.

Table 4. Stoner product $I \cdot N_d(E_F)$ for the d-projected density of states of every inequivalent metal site, using representative atomic Stoner exchange parameters from Janak (1977): I(Ti) ≈ 0.24 eV, I(Mo) ≈ 0.29 eV. $N_d(E_F)$ is the spin-averaged d-projected density of states per atom per spin channel, used here as a proxy for the corresponding non-spin-polarized value given the near-mirror-symmetric spin channels established in Section 3.4.

Compound	M site	$N_d(E_F)$ (states/eV/atom)	$I \cdot N_d(E_F)$
Ti_2AlC	Ti	0.1658	0.0398
Ti_3AlC_2	Ti1	0.1215	0.0292
Ti_3AlC_2	Ti2	0.1694	0.0407
Ti_4AlC_3	Ti1	0.1580	0.0379
Ti_4AlC_3	Ti2	0.0849	0.0204
Mo_2AlC	Mo	0.2923	0.0847
Mo_3AlC_2	Mo1	0.4713	0.1367
Mo_3AlC_2	Mo2	0.4664	0.1352
Mo_4AlC_3	Mo1	0.3975	0.1153
Mo_4AlC_3	Mo2	0.3441	0.0998

The clearest confirmation of this argument sits inside the MAX-phase literature itself, not outside it. $Mo_{0.5}Mn_{0.52}GaC$ is magnetic, and the ordered moment resides predominantly on the manganese sublattice rather than being shared equally with molybdenum (Meshkian et al., 2015), providing direct, compound-level evidence that molybdenum's own electronic character does not favor local-moment formation in this structural family, even when it shares a unit cell with an element that does. Titanium tells the same story on its own terms: every Ti-based MAX phase examined here, Ti_2AlC, Ti_3AlC_2, and Ti_4AlC_3, is non-magnetic, and nothing about adding further Ti-C layers changes that. The chemistry that produces magnetism in this family is specific, narrow, favorably filled, exchange-favorable d bands, the kind Mn supplies and Ti and Mo do not, rather than a generic property of the $M_{n+1}AX_n$ structure that any transition metal could, in principle, trigger.

3.6. Practical implications of confirmed non-magnetism

The confirmed non-magnetic character of all six compounds is a favorable attribute for the high-temperature structural, protective-coating, electrical-contact, and thermoelectric applications typically envisaged for MAX phases. On the evidence assembled here, none of the six compounds is expected to show a Curie-point anomaly in resistivity or thermal expansion, an additional magnon contribution to thermal transport, or magnetostrictive coupling between mechanical deformation and the magnetic state; these are expectations that follow from the confirmed absence of a magnetic ground state rather than properties measured directly in this work, since no finite-temperature transport or elastic calculation was performed here. This distinction matters in particular for Mo_3AlC_2, Mo_4AlC_3, and Ti_4AlC_3, which, as noted in Section 1, remain hypothetical structural models without a confirmed phase-pure bulk synthesis; the non-magnetic conclusion reached for them applies to the assumed 211/312/413 structural prototype, and any application-relevant statement about these three compounds should be read with that caveat attached. Beyond this specific family, the result also supports a broader methodological choice for our companion, non-spin-polarized transport studies of these same six compounds (Sirati-Gohari et al., in press-a; Sirati-Gohari et al., in press-b), precisely because the magnetic assumption those studies depend on has been checked explicitly here for all six compounds, rather than inherited by default.

3.7. Chromium as a contrasting case, and outlook across the M-site

The three-criteria framework applied here to molybdenum and titanium is, by construction, chemistry-agnostic, and it is natural to ask how it would read for an M-site element known to sit closer to the magnetic instability. Chromium is the obvious test: it sits directly adjacent to manganese, and some chromium-containing MAX phases already show measurable low-temperature moments experimentally (Jaouen et al., 2014), while computational studies disagree on the sign and size of the effect depending on the level of theory (Dahlqvist, Alling, & Rosén, 2015; Dahlqvist & Rosén, 2020; Ingason, Dahlqvist, & Rosén, 2016).

We did not carry out the full three-criteria protocol for chromium, and we make no quantitative magnetic-moment claim for a Cr-based MAX phase in this paper; that is left, together with vanadium and niobium, to a dedicated follow-up study. What we can report here, using the same spin-polarized DOS calculation already performed for Cr_2AlC as part of a related project, is a direct, qualitative contrast against the third criterion used throughout this work. Whereas the spin-up and spin-down total and d-projected densities of states of all six Mo- and Ti-based compounds are near-perfect mirror images of one another (Section 3.4, Figure 3), the corresponding spin-up and spin-down densities of states of Cr_2AlC are visibly and substantially asymmetric: the Cr *3d*-projected density of states at E_F is roughly 1.05 states/eV/atom in the spin-up channel against roughly 0.58 states/eV/atom in the spin-down channel, an imbalance of the order of 45%, some forty to fifty times larger than the sub-1% asymmetry reported for every Mo- and Ti-based compound in Table 3. This is precisely the qualitative signature that Section 3.4 identifies as the fingerprint of genuine exchange splitting rather than numerical noise, and it is consistent with the mixed but non-trivial experimental and computational record for chromium-based MAX-phase magnetism already noted above (Jaouen et al., 2014; Dahlqvist, Alling, & Rosén, 2015; Ingason, Dahlqvist, & Rosén, 2016). Taken together with the uniformly mirror-symmetric behavior of the six compounds that are the subject of this paper, this contrast supports the view that the magnetic behavior of the chromium-based M_2AlC series is qualitatively distinct from that of its molybdenum- and titanium-based neighbors, and that it warrants the dedicated, full three-criteria treatment, including the antiferromagnetic and noncollinear configurations outside the scope of the present collinear study, that we plan as independent future work.

Extending the present protocol to vanadium and niobium as well would complete a systematic, M-site-resolved map of magnetic tendency across the early transition-metal M_2AlC series, anchored at one end by the confirmed non-magnetic Ti- and Mo-based compounds established here and, at the other, by the confirmed magnetic Mn-containing compounds already reported in the literature, with chromium occupying the intermediate, still-unsettled position that the contrast above suggests.

4. Conclusions

In this work, we asked a simple question: can we safely assume that molybdenum- and titanium-based MAX phases are non-magnetic? We tested this assumption for six compounds, Mo_2AlC, Mo_3AlC_2, Mo_4AlC_3, Ti_2AlC, Ti_3AlC_2, and Ti_4AlC_3, using three independent criteria, supplemented by a quantitative Stoner-product check. The criteria agree with each other. First, the converged spin moments of all six compounds are negligible, and no inequivalent atomic site carries a local moment inconsistent with numerical noise. Second, the spin-polarized total energy is not systematically lower than the non-spin-polarized one: four of the six compounds show the numerically forbidden, positive-ΔE sign expected of residual noise rather than of a real spin instability, and none shows the large, systematically negative ΔE a genuine Stoner instability would require. Third, the density of states at the Fermi level shows no resolvable exchange splitting, either across the full valence range or in an expanded view around E_F, and the explicit Stoner estimate, $I \cdot N_d E_F$), remains below 0.14 at every metal site studied, an order of magnitude short of the ferromagnetic instability threshold. In other words, within the collinear, spin-orbit-free framework adopted here, all six MAX phases are Pauli paramagnets; this study does not rule out a compensated antiferromagnetic or noncollinear ground state, although the site-resolved local moments of Table 2 show no pattern suggestive of one.

Why are these compounds non-magnetic? The answer lies in their electronic structure. The d bands of molybdenum and titanium are broad and strongly hybridized. As a result, they do not develop a high density of states at the Fermi level, which is the condition needed for magnetism according to the Stoner criterion. This behavior differs sharply from manganese-containing MAX phases, whose narrower, more favorably filled d states can favor spin polarization, and it differs, more subtly but measurably, from the substantially spin-asymmetric density of states we find for chromium, the M-site element that sits closest to the manganese-driven instability among those considered here.

This work carries a practical message. The non-magnetic approximation is valid for these compounds within the scope tested here, but it should not be assumed without testing, and for the three compounds without a confirmed bulk synthesis, Mo_3AlC_2, Mo_4AlC_3, and Ti_4AlC_3, it should be read as a statement about the assumed structural model rather than about a confirmed ground-state phase. Verifying the magnetic ground state is cheap and fast compared with full property calculations, and it protects later studies, including our own companion transport studies of these same six compounds, from building on a wrong starting point. The same check can be extended to chromium, vanadium, and niobium, where our own preliminary chromium data already point toward qualitatively different behavior and motivate a dedicated, full antiferromagnetic and noncollinear treatment as independent future work. We hope this straightforward, quantitatively anchored workflow helps the community verify the magnetic ground state of MAX phases more routinely.

Data Availability

The WIEN2k input and output files (structure files, self-consistent-field output for the spin-polarized and non-spin-polarized calculations, and density-of-states files) generated and analyzed in this study are available from the corresponding authors upon reasonable request.

CRediT Author Statement

Maryam Sirati-Gohari: Conceptualization, Data Curation, Formal Analysis, Investigation, Methodology, Software, Validation, Visualization, Writing – original draft, Writing – review & editing. Sirus Javadpour: Conceptualization, Data Curation, Formal Analysis, Funding Acquisition, Investigation, Project Administration, Resources, Supervision, Validation. Mohammad Mahdi Kalantarian: Conceptualization, Data Curation, Formal Analysis, Funding Acquisition, Investigation, Methodology, Project Administration, Resources, Software, Supervision, Validation, Visualization, Writing – original draft, Writing – review & editing. Alimorad Rashidi: Data Curation, Formal Analysis, Investigation, Resources, Supervision, Validation. Touradj Ebadzadeh: Data Curation, Formal Analysis, Investigation, Resources, Supervision, Validation

Declaration of Competing Interest

The authors declare that they have no known competing financial interests or personal relationships that could have appeared to influence the work reported in this paper.

Acknowledgment

This study is derived from the PhD student project of Maryam Sirati-Gohari. This work is based upon research funded by Iran National Science Foundation (INSF) under project No 40402001.

REFERENCES

1. Ali, M. S., Rayhan, M. A., Ali, M. A., Parvin, R., & Islam, A. K. M. A. (2016). New MAX phase compound Mo2TiAlC2: First-principles study. Journal of Scientific Research, 8, 109–117. https://doi.org/10.3329/jsr.v8i2.25057

2. Anasori, B., Dahlqvist, M., Halim, J., Moon, E. J., Lu, J., Hosler, B. C., Caspi, E. N., May, S. J., Hultman, L., Eklund, P., Rosén, J., & Barsoum, M. W. (2015). Experimental and theoretical characterization of ordered MAX phases Mo2TiAlC2 and Mo2Ti2AlC3. Journal of Applied Physics, 118, 094304. https://doi.org/10.1063/1.4929640

3. Barsoum, M. W. (2000). The Mn+1AXn phases: A new class of solids: Thermodynamically stable nanolaminates. Progress in Solid State Chemistry, 28, 201–281. https://doi.org/10.1016/S0079-6786(00)00006-6

4. Barsoum, M. W. (2013). MAX phases: Properties of machinable ternary carbides and nitrides. Wiley-VCH. https://doi.org/10.1002/9783527654581

5. Barsoum, M. W., & Radovic, M. (2011). Elastic and mechanical properties of the MAX phases. Annual Review of Materials Research, 41, 195–227. https://doi.org/10.1146/annurev-matsci-062910-100448

6. Blaha, P., Schwarz, K., Tran, F., Laskowski, R., Madsen, G. K. H., & Marks, L. D. (2020). WIEN2k: An APW+lo program for calculating the properties of solids. Journal of Chemical Physics, 152, 074101. https://doi.org/10.1063/1.5143061

7. Cover, M. F., Warschkow, O., Bilek, M. M. M., & McKenzie, D. R. (2009). A comprehensive survey of M2AX phase elastic properties. Journal of Physics: Condensed Matter, 21, 305403. https://doi.org/10.1088/0953-8984/21/30/305403

8. Dahlqvist, M., & Rosén, J. (2020). Impact of strain, pressure, and electron correlation on magnetism and crystal structure of Mn2GaC from first-principles. Scientific Reports, 10, 11396. https://doi.org/10.1038/s41598-020-68377-5

9. Dahlqvist, M., Alling, B., & Rosén, J. (2010). Stability trends of MAX phases from first principles. Physical Review B, 81, 220102. https://doi.org/10.1103/PhysRevB.81.220102

10. Dahlqvist, M., Alling, B., & Rosén, J. (2015). A critical evaluation of GGA+U modeling for atomic, electronic and magnetic structure of Cr2AlC, Cr2GaC and Cr2GeC. Journal of Physics: Condensed Matter, 27, 095601. https://doi.org/10.1088/0953-8984/27/9/095601

11. Ingason, A. S., Dahlqvist, M., & Rosén, J. (2016). Magnetic MAX phases from theory and experiments: A review. Journal of Physics: Condensed Matter, 28, 433003. https://doi.org/10.1088/0953-8984/28/43/433003

12. Ingason, A. S., Mockute, A., Dahlqvist, M., Magnus, F., Olafsson, S., Arnalds, U. B., Alling, B., Abrikosov, I. A., Hjörvarsson, B., Persson, P. O. Å., & Rosén, J. (2013). Magnetic self-organized atomic laminate from first principles and thin film synthesis. Physical Review Letters, 110, 195502. https://doi.org/10.1103/PhysRevLett.110.195502

13. Ingason, A. S., Petruhins, A., Dahlqvist, M., Magnus, F., Mockute, A., Alling, B., Hultman, L., Abrikosov, I. A., Rosén, J., & Persson, P. O. A. (2014). A nanolaminated magnetic phase: Mn2GaC. Materials Research Letters, 2, 89–93. https://doi.org/10.1080/21663831.2013.865105

14. Janak, J. F. (1977). Uniform susceptibilities of metallic elements. Physical Review B, 16, 255–262. https://doi.org/10.1103/PhysRevB.16.255

15. Jaouen, M., Bugnet, M., Jaouen, N., Ohresser, P., Mauchamp, V., Cabioc'h, T., & Rogalev, A. (2014). Experimental evidence of Cr magnetic moments at low temperature in Cr2A (A = Al, Ge)C. Journal of Physics: Condensed Matter, 26, 176002. https://doi.org/10.1088/0953-8984/26/17/176002

16. Lashgari, E., Kalantarian, M. M., Yousefi-Mashhour, H., Sirati-Gohari, M., Ahmadkhan Kordbacheh, A., Eshraghi, M. J., & Omidvar, H. (2026). Ab-initio evaluation of V2O5 as the electrode of intercalation batteries. Materials Today Communications, 54, 115513. https://doi.org/10.1016/j.mtcomm.2026.115513

17. Kalantarian, M. M., Asgari, S., & Mustarelli, P. (2013). Theoretical investigation of Li2MnSiO4 as a cathode material for Li-ion batteries: A DFT study. Journal of Materials Chemistry A, 1, 2847–2855. https://doi.org/10.1039/C2TA01363K

18. Khazaei, M., Arai, M., Sasaki, T., Estili, M., & Sakka, Y. (2014). Trends in electronic structures and structural properties of MAX phases: A first-principles study on M2AlC (M = Sc, Ti, Cr, Zr, Nb, Mo, Hf, or Ta), M2AlN, and hypothetical M2AlB phases. Journal of Physics: Condensed Matter, 26, 505503. https://doi.org/10.1088/0953-8984/26/50/505503

19. Meshkian, R., Ingason, A. S., Dahlqvist, M., Petruhins, A., Arnalds, U. B., Magnus, F., Alling, B., & Rosén, J. (2015). A magnetic atomic laminate from thin film synthesis: (Mo0.5Mn0.5)2GaC. APL Materials, 3, 076102. https://doi.org/10.1063/1.4926611

20. Monkhorst, H. J., & Pack, J. D. (1976). Special points for Brillouin-zone integrations. Physical Review B, 13, 5188–5192. https://doi.org/10.1103/PhysRevB.13.5188

21. Perdew, J. P., Burke, K., & Ernzerhof, M. (1996). Generalized gradient approximation made simple. Physical Review Letters, 77, 3865–3868. https://doi.org/10.1103/PhysRevLett.77.3865

22. Shahpouri, E., Hassani, S., Yousefi-Mashhour, H., Kalantarian, M. M., Ebadzadeh, T., & Mobasherpour, I. (2024). Evaluation of Ti3C2 as electrode material for Li, Na, Mg, Al, K, Ca, and Zn-ion intercalation batteries: A DFT study. Results in Chemistry, 7, 101385. https://doi.org/10.1016/j.rechem.2024.101385

23. Shahpouri, E., Kalantarian, M. M., Ebadzadeh, T., & Mobasherpour, I. (2025). Investigation on titanium-based MXenes in Li-ion batteries: Empowering future electrodes. Applied Surface Science, 689, 162524. https://doi.org/10.1016/j.apsusc.2025.162524

24. Shahpouri, E., Kalantarian, M. M., Ebadzadeh, T., & Mobasherpour, I. (2026). MXene M2C (M = Ti, V, Cr, and Nb) as electrode material for various intercalation batteries (Li, Na, Mg, Al, K, Ca, and Zn-ion): Ab-initio studies. Surfaces and Interfaces, 80, 108174. https://doi.org/10.1016/j.surfin.2025.108174

25. Sirati-Gohari, M., Javadpour, S., Kalantarian, M. M., Rashidi, A., & Ebadzadeh, T. (in press-a). Rigid-band doping engineering of the thermoelectric power factor in molybdenum and titanium-based MAX-phases.

26. Sirati-Gohari, M., Javadpour, S., Kalantarian, M. M., Rashidi, A., & Ebadzadeh, T. (in press-b). Doping-tunable transport anisotropy and direction-dependent Seebeck in Mo- and Ti-based MAX-phases.

27. Stoner, E. C. (1938). Collective electron ferromagnetism. Proceedings of the Royal Society A, 165, 372–414. https://doi.org/10.1098/rspa.1938.0066

28. Sun, Z. M. (2011). Progress in research and development on MAX phases: A family of layered ternary compounds. International Materials Reviews, 56, 143–166. https://doi.org/10.1179/1743280410Y.0000000001

29. Togo, A., & Tanaka, I. (2015). First principles phonon calculations in materials science. Scripta Materialia, 108, 1–5. https://doi.org/10.1016/j.scriptamat.2015.07.021

30. Yousefi-Mashhour, H., Hassani, S., Momeni, M., Kalantarian, M. M., & Namiranian, A. (2024). Insight into behaviors and properties of AMO2 (A = Na and Li; M = Mn, Fe, Co, Ni, and Ni1/3Co1/3Mn1/3) cathode materials: A DFT evaluation. Results in Chemistry, 7, 101348. https://doi.org/10.1016/j.rechem.2024.101348

31. Yousefi-Mashhour, H., Kalantarian, M. M., & Namiranian, A. (2023). Effect of fluorine doping on LiCoO2 cathode material: A DFT study. Advanced Ceramics Progress, 9(4), 15–21. https://doi.org/10.30501/acp.2023.425848.1139

32. Zamani, K., Tavoosi, M., Ghasemi, A., & Gordani, G. (2023). Structural and phase stability in the 2TiC-Al-Ti system during milling and subsequent annealing. Advanced Ceramics Progress, 9(4), 41–49. https://doi.org/10.30501/acp.2024.431563.1142